Cobalt Electrodeposition in Nanoporous Anodic Aluminium Oxide Films with Different Oxidation Time

Di MA [1] *, Shubai LI [2], Dongmei YU [1], Xinyu LYU [3], Bin WANG [1], Zou CHEN [1], Danan HOU [1]

[1] *School of Chemistry & Environmental Engineering, Jiangsu University of Technology, 1801 Zhongwu Rd., Changzhou, Jiangsu, 213001 China*
[2] *Department of Chemical Engineering, Changzhou Institute of Engineering Technology, 33 Gehu Middle Rd., Changzhou, Jiangsu, 213164 China*
[3] *Jiangsu Key Laboratory of Advanced Catalytic Materials and Technology, Changzhou University, Yanzheng West Rd., Changzhou, Jiangsu, 213164 China*

The anodic aluminum oxide films with different oxidation times were investigated using electrochemical techniques including electrochemical impedance spectroscopy (EIS), cyclic voltammetry (CV), and open-circuit potential versus time. The stable open-circuit potential versus time indicates that the longer anodization time provides a larger block for cobalt electrodeposition. The EIS monitoring revealed the capacitance characteristics of the barrier layer. When the oxidation time is 4 h, the thickness and porosity of AAO film are 1517 nm and 16.4 % correspondingly, and the radius of the capacitive reactance arc is the smallest. The reduction peak current of CV is attributed to the change in diffusion coefficient of cobalt when oxidation time changes.

Keywords: anodic aluminum oxide template, electrodeposition, cobalt, nanoporous.

1. INTRODUCTION

The template method is an important means for synthesizing nanowire materials, and its spatial confinement and structure guiding characteristics can be used to effectively modulate the size, morphology, and structure of the material.

The structure of porous anodized aluminum oxide (AAO) is determined by structural parameters, such as pore spacing, pore diameter, the barrier layer, porous layer thickness, pore density, and porosity. The structural parameters are taken from the oxidation conditions: electrolyte type, oxidation voltage, current density, temperature, etc [1 – 3]. A highly ordered one-dimensional nanomaterial can be prepared using the template method combined with electrochemical deposition, chemical vapor deposition, sol-gel, and other methods [4, 5]. The AAO template has the characteristics of simple process flow, adjustable pore size, and thickness of the template, so it is an ideal template for the synthesis and assembly of nanomaterials [1, 6].

The AAO template has recently attracted considerable attention in the fabrication of nanostructures used in electronic optoelectronic devices, optics, magnetics, and catalysis [7 – 15], because of its highly ordered arrangement.

However, the application of the AAO structure as a catalyst framework is still an interesting but rarely studied area. The function of heterogeneous catalysts mainly depends on their structure on a series of length scales [16 – 19].

By using a series of nanoreactors produced using an AAO structure with highly ordered nanopores, the reactants must flow through the nanopores, which makes these pores function as nanoscale reactors [20 – 22]. The pore size and length are controllable, so the one-dimensional channel structure is conducive to the deposition of precious metal particles and catalytically active materials [22].

In this work, we propose an approach for electrodepositing cobalt in porous anodic aluminum oxide (AAO) with different anodizing times. With the increase of oxidation time, the pores of the AAO template will change, resulting in a change in the electrodeposition process. It is helpful to understand the deposition process of cobalt in the AAO template. AAO templates were prepared in phosphoric acid solution and characterized by micro-morphology characterization and electrochemical methods. The effects of oxidation time on the performance and morphology of AAO templates after cobalt deposition were investigated.

2. EXPERIMENTAL DETAILS

A high pure (99.999%) Al foil of 0.2 mm thickness was ultrasonically degreased in ethanol for 180 s and etched in 1.5 mol l^{-1} NaOH at 60 °C for 30 s, rinsed thoroughly with deionized water. Anodization was performed in 0.4 mol/L H_3PO_4 aqueous solutions at a constant voltage of 80 V for 1 h at 4 °C. After the first anodization, the anodic aluminum oxide (AAO) template was removed immersing in a 20 g/L CrO_3 and 35 ml/L H_3PO_4 mixture at 60 °C for 5 h. Observe and confirm that the once anodized aluminum sheet is completely removed, and then the second anodization was performed under the same andic conditions.

---

* Corresponding author. Tel.: +86-15951207428.
E-mail address: *madi@jsut.edu.cn* (Di Ma)

Cobalt was electrodeposited into the pores of AAO templates using a three-electrode cell. The AAO template with the unstripped aluminum substrate is used as the working electrode, a palate sheet was used as the counter electrode. The electrodeposition of cobalt was carried out in a solution of 8.4 g/L $CoSO_4$ and 30 g/L H_3BO_3, at room temperature and 10 min with a current density of 15 mA at 50 Hz. The TAFEL diagrams, Cyclic Voltammogram (CV), and electrochemical impedance spectroscopy (EIS) are tested by the CHI 660C electrochemical system. The scan rate of CV is 0.01 Vs^{-1}, and the oscillation potential of EIS is 10 mV. The microstructure of the AAO template was characterized by a scanning electron microscope (SEM) (SEM, Hitachi S-3400NII).

3. RESULTS AND DISCUSSION

Morphology of the cross-sections of AAO templates formed by different oxidation times and Co synthesized within AAO pores are shown in Fig. 1. The oxidation time of Fig. 1 a–d is 1 h, 2 h, 3 h, and 4 h respectively, and the corresponding AAO template thickness is 689 nm, 976 nm, 1766 nm, and 1517 nm. It can be seen from the figure that the AAO template has a uniform and dense structure, with smooth channels and no cross phenomenon. The bending part is caused by the stress during the preparation of the test sample, and the layered structure is arranged neatly along the growth direction of the template, which is formed by the fracture of the channels during the longitudinal cutting of the AAO template. The template has a stable structure and high pore density, which is suitable for the electrodeposition of Co nanowires.

According to the formation theory of AAO film [23], the barrier layer continues to form and dissolve at the pore base, the thickness of the barrier layer does not change, and the porous layer begins to thicken. Therefore, the AAO film thickness gradually increases as the oxidation time increases. But when the characteristic time is reached, the film thickness no longer increases, reaching the limit thickness. As the oxidation time continues to prolong, the surface of the AAO film will be partially chemically dissolved in the electrolyte, so the film thickness decreases slightly. This is similar to that observed by Pattermarakis [24] and Shawaqfeh [25] that the thickness of AAO formed in sulfuric acid and phosphoric acid solutions varies with oxidation time. Fig. 2 shows SEM images and the pore diameter distribution of the AAO template sample anodized at different times. The statistical nature of this analysis provides an opportunity to understand the pore diameter distribution (Fig. 1). The influence of an anodization time on the Feret's diameter, pore density, and porosity of the AAO template was obtained through the statistical analysis of SEM images by ImageJ software, which is listed in Table 1.

Table 1. Statistical parameters of Ag colloidal solution

Oxidation time, h	Feret's diameter, nm	Pore density, number/µm²	Porosity, %
1	32	32	10.1
2	55	25	11.3
3	54	15	17.4
4	92	21	16.4

a   b   c   d

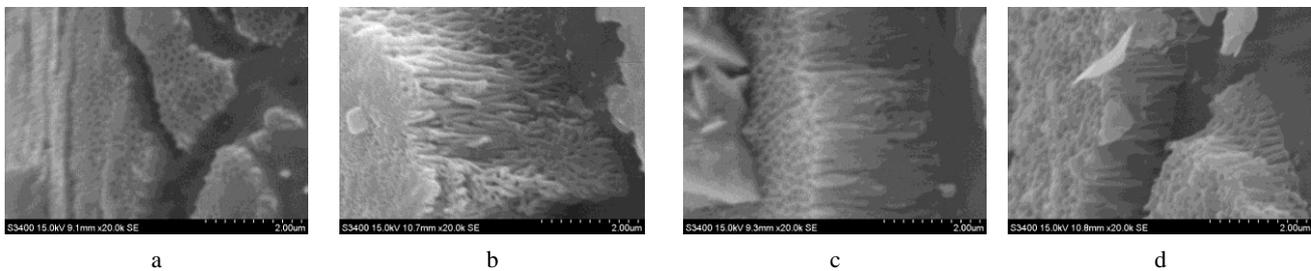**Fig. 1.** Scanning electron microscopy of AAO template with different oxidation time

a   b   c   d
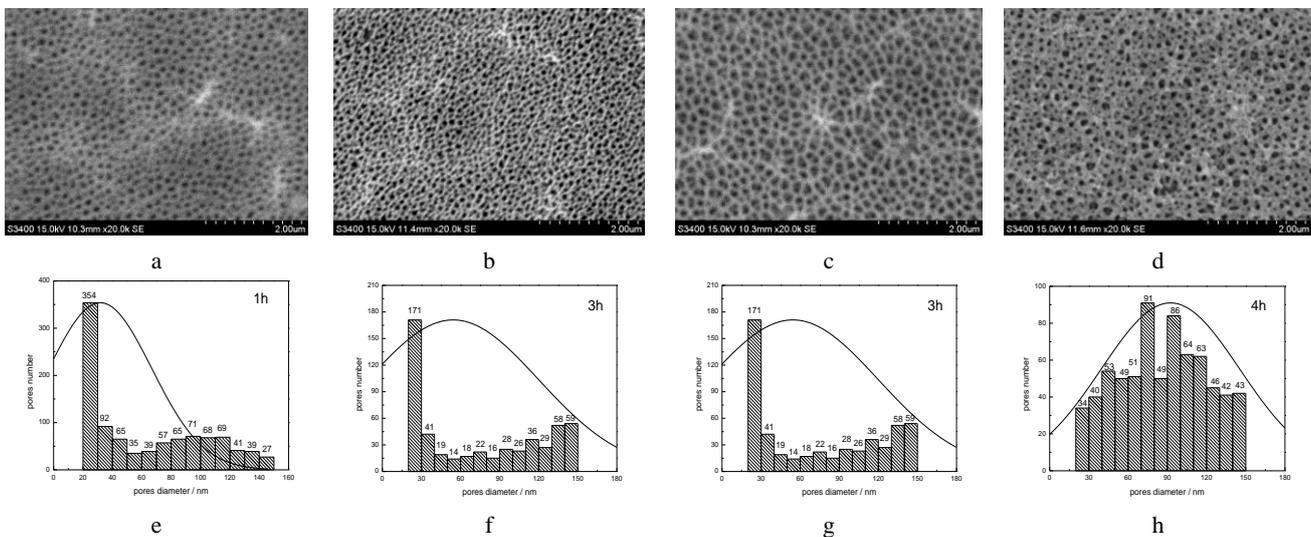

e   f   g   h

Fig. 2. SEM images and the pore diameter distribution of the AAO template sample anodized: a, e – 1 h; b, f – 2 h; c, g – 3 h; d, h – 4 h

The Feret's diameter in AAO samples exclusively comprised the smaller pore classes (30–100 nm). The porosity observed in the AAO samples: porosity larger than 17.4 % is found, as well as pores in the 10–17 % ranges. The larger pores in the microstructure also reflect a larger porosity (Table 1). The porosity volume fraction and Feret's diameter of the AAO samples represent an increase with the increase of anodization time. With the extension of oxidation time and the increase of immersion time in acid, the surface of the film dissolves, which first occurs around the pores, increasing surface pore size and porosity [26].

Fig. 3 shows the change of open circuit potential with time for the AAO template sample oxidized at a different time exposed to 0.1 mol / L cobalt salt solution. The open potential is immediately dropped from -0.52 V to -0.39 V from 0 s to 245 s and gradually decreases to -0.5 V versus Ag/AgCl (the anodization time is 1 h). The stable OCP(Open Circuit Potential) of the AAO template with an anodizing time of 1 h, when compared with the stable OCP at -0.5 V for the AAO template with a longer anodizing time in the same solution (the anodizing time of 2, 3, 4 h), indicates that the longer anodization time provides a larger block for cobalt electrodeposition. In contrast, the OCP for the AAO template with the anodizing time of 1 h was fluctuating and never stable. The OCP fluctuations are associated with the onset of pores of the template and the blocking of the nanoholes by cobalt ions.
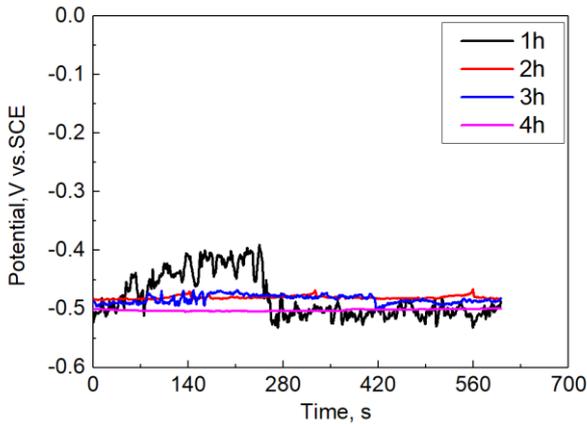

Fig. 3. OCP vs. time for the AAO template sample anodized at a different time exposed to 0.1 mol / L cobalt salt solution

Fig. 4 shows Nyquist plots of EIS spectra for the AAO template sample anodized at the different times exposed to 0.1 mol / L cobalt salt solution. The spectra obtained are similar under different oxidation times. There are relatively complete capacitive reactance arcs in the low-frequency and high-frequency regions of the impedance spectrum under different oxidation times. In the first arc, the capacitive reactance arc is the largest when the oxidation time is 2 h, and the capacitive reactance arc is the smallest when the oxidation time is 3 h; in the second arc, with the decrease of frequency, the imaginary part of the curve impedance with oxidation time of 3 h starts to be larger than that with oxidation time of 2 h. When the real part of the impedance is about 200 ohm, the capacitive arc with oxidation time of 1 h is the largest; when the oxidation time is 4 h, the curve is concentrated in the high-frequency

region, the second arc is a capacitive semicircle, and the capacitive arc is the smallest in all curves. When the real part of the impedance is about 200 ohm, the capacitive arc with oxidation time of 1 h is the largest; when the oxidation time is 4 h, the curve is concentrated in the high-frequency region, the second arc is a capacitive semicircle, and the capacitive arc is the smallest in all curves.
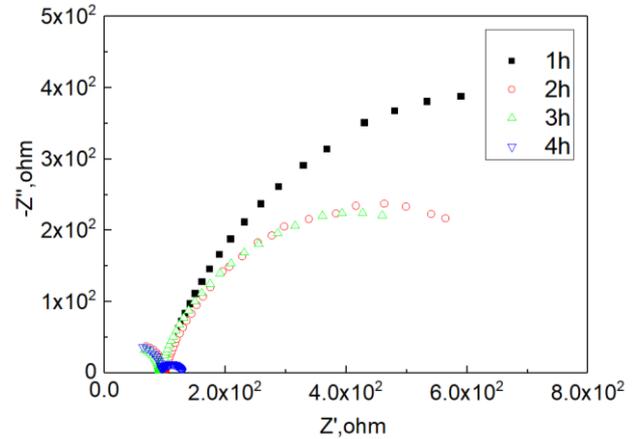
Fig. 4. The Nyquist diagrams of EIS spectra for the AAO template sample were prepared at different anodization time (1 h, 2 h, 3 h, and 4 h)

The proposed equivalent electrical circuit is shown in Fig. 3. Anodic aluminum oxide coating's response to EIS measurements has been broadly studied for decades. The equivalent circuit is shown in Fig. 5. The description code of its equivalent circuit is $R (QR) (QR)$. R_S is the resistance of electrolyte solution; R_p and CPE_p is a resistance and a constant phase element associated with the sealing of the pores; R_b and CPE_b is a resistance and a constant phase element associated with the barrier layer. The parameters of each element calculated by Zsimpwin software are listed in Table 2.
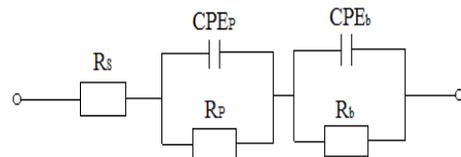

Fig. 5. The equivalent electrical circuit used to model impedance data in the case of the AAO template sample

Table 2 shows the values of the different impedance parameters of the AAO template sample. It is evident from Table 1 that the value of polarization resistance significantly increases with the oxidation time. The solution resistance R_s and the resistance R_p of the porous layer have no obvious change, R_s is stable at about 18 Ω, and R_p is stable at about 78 Ω. The resistance R_b of the barrier layer is decreased from 1025 Ω to 33.75 Ω as the anodization time increases from 1 to 4 h, confirming the decreasing barrier layer thickness of the AAO template. Because most of the n_b is close to 1, that is, CPE_b is close to the ideal situation, which can be a good substitute for capacitance. The impedance characteristics of composite elements mainly reflect the capacitance characteristics of the barrier layer, which can be related to the thickness of the barrier layer by the following formula:

Table 2. Impedance parameters of the AAO template sample prepared at different anodization times (1 h, 2 h, 3 h, and 4 h)

Oxidation time, h	R_S, Ω	R_P, Ω	R_b, Ω	n_p	CPE$_P$, S-sec^n	n_b	CPE_b, S-sec^n
1	19.51	78.18	1025.00	0.94	2.94×10^{-8}	0.81	2.35×10^{-4}
2	18.15	81.65	1492.00	0.96	3.19×10^{-8}	0.82	1.33×10^{-4}
3	18.49	72.54	604.60	0.96	3.35×10^{-8}	0.79	2.97×10^{-4}
4	15.40	79.27	33.75	0.95	3.57×10^{-8}	0.82	1.55×10^{-4}

$$C_b = \frac{\varepsilon \varepsilon_0 S}{\delta_b}, \tag{1}$$

where ε is the dielectric constant of the anodic oxide film with a value of 10; ε_0 is the dielectric constant of vacuum with a value of 8.854×10^{-12} F/m; $S = 1$ cm^2, which is the surface area of the electrode. It can be calculated that when the oxidation time is 1 to 4 h, as the oxidation time is extended, the thickness of the barrier layer becomes thinner after electrodeposition.

In the Bode diagram (Fig. 6), from the relationship between frequency and mode value, in the frequency range of $10^{-1} \sim 10^2$ Hz, the larger the mode value is, which corresponds to the decrease of the thickness of the barrier layer mentioned above. During the oxidation time of $3-4$ h, the mode value decreases sharply; in the frequency range of $10^2 \sim 10^6$ Hz, the anodic oxidation time has no obvious effect on the mode value in a frequency range, and the curves coincide with each other. There is only one peak of phase angle in the four figures, which indicates that the system has only one relaxation time and the electrochemical process has only a one-speed control step. Because the electrolyte can directly contact the impedance layer, the resistance R_P of the porous layer is too small compared with the resistance R_b of the barrier layer due to its strong conductivity.
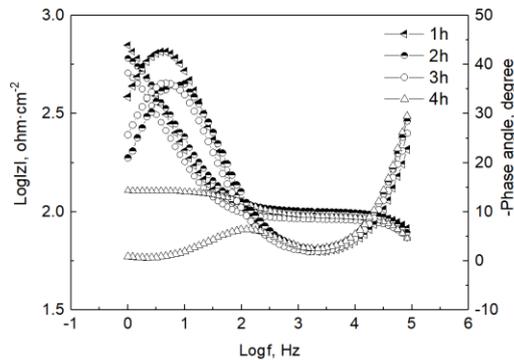
Fig. 6. The Bode diagrams of EIS spectra for the AAO template sample were prepared at different anodization times (1 h, 2 h, 3 h, and 4 h)

Cyclic voltammetry measurements were carried out on an AAO sample for Co electrodeposition from 0.1 mol / L cobalt salt bath at a scanning rate of 0.01 V / s. (Fig. 7). The cathodic current appears from -0.7 V in all four curves. There is a reduction current peak and an oxidation current peak on the CV Curve. The reduction current peak corresponds to the deposition of cobalt, and the oxidation current peak corresponds to the dissolution of cobalt. When the oxidation time was 1 h and 2 h, with the extension of oxidation time, the oxidation peak current decreased from 10.51 mA to 7.08 mA, the reduction peak current decreased from -4.52 mA to -0.65 mA, the reduction peak current shifted to the negative potential direction, and the oxidation peak position remained unchanged.
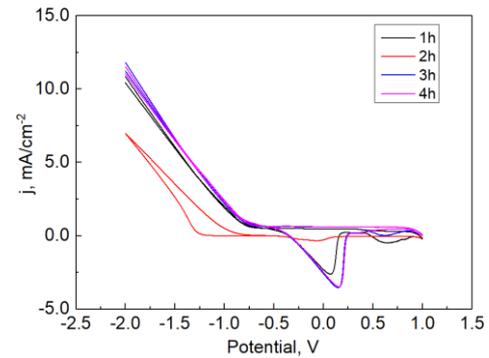
Fig. 7. Cyclic voltammograms of the AAO template sample anodized at different times (1 h, 2 h, 3 h, and 4 h) exposed to 0.1 mol / L cobalt salt solution

When the oxidation time is 3 h and 4 h, with the extension of oxidation time, the oxidation peak current decreases from 11.22 mA to 10.99 mA, the reduction peak current decreases from -5.66 mA to -5.13 mA, the reduction peak current also moves to the negative potential direction, and the oxidation peak position is unchanged.

4. CONCLUSIONS

The impact of the anodization time of AAO on the electrodeposition of Co was studied. From the analysis of the AC impedance spectrum and equivalent circuit, it can be seen that AC impedance mainly reflects the capacitance characteristics of the barrier layer. When the oxidation time is 4 h, the radius of the capacitive reactance arc is the smallest and the thickness of the barrier layer is the thinnest. The cyclic voltammetry test shows that the change of reduction peak current is attributed to the change of diffusion coefficient of cobalt when oxidation time changes. The reduction peak current is -5.66 mA when oxidation time is 3 h and -5.13 mA when oxidation time is 4 h. the corresponding reduction peak area is larger in both cases.

The characterization of the template by SEM and ImageJ software shows that the pore size distribution on the surface of the template is the most uniform after oxidation for 4 h, and the Feret's diameter is 92 nm. At this time, the pore size is the largest, and the thickness of the template is 1517 nm, which is second only to oxidation for 3 h. the surface of the template is smooth, with fewer voids and no cross channels, which meets the requirements of cobalt deposition. In conclusion, the

deposition effect is the best when the oxidation time is 4 h.

REFERENCES

1. **Young, L.** Anodic Oxide Films. New York: Academic Press, 1961.

2. **Hoar, T.P.** The Anodic Behaviour of Metals *Corrosion Science* 341 (7) 1967: pp. 341 – 355.

3. **Takahashi, H., Nagayama, M.** Electrochemical Behavior and Structure of Anodic Oxide Films Formed on Aluminum in A Neutral Borate Solution *Electrochimica Acta* 23 (3) 1978: pp. 279 – 286.
https://doi.org/10.1016/0013-4686(78)85058-0

4. **Masuda, H., Asoh, H., Watanabe, M.W., Nishio, K., Tamamura, T.** Square and Triangular Nanohole Array Architectures in Anodic Alumina *Advanced Materials* 13 (3) 2001: pp. 189 – 192.
https://doi.org/10.1002/1521-4095(200102)13

5. **Masuda, H., Fukuda, K.** Ordered Metal Nanohole Arrays Made by a Two-Step Replication of Honeycomb Structures of Anodic Alumina *Science* 268 (5216) 1995: pp. 1466 – 1468.
https://doi.org/10.1126/science.268.5216.1466

6. **Renshaw, T.** A Study of Pore Structures on Anodized Aluminum *Journal of the Electrochemical Society* 108 (2) 1961: pp. 185 – 191.
https://doi.org/10.1149/1.2428038

7. **Liu, Y., Zhang, K., Li, M., Zhao, C., Wang, X., Yuan, Z.** Ion Emission Properties of Indium Nanowires Grown on Anodic Aluminum Oxide Template *Vacuum* 131 2016: pp. 209 – 212.
https://doi.org/10.1016/j.vacuum.2016.06.019

8. **Nguyen, V.H., Kato, S., Usami, N.** Evidence for Efficient Passivation of Vertical Silicon Nanowires by Anodic Aluminum Oxide *Solar Energy Materials and Solar Cells* 157 2016: pp. 393 – 398.
https://doi.org/10.1016/j.solmat.2016.07.002

9. **Selvamurugan, V., Mangamma, G., Ravi, S., Kamruddin, M., Madhavan, D., Marikani, A.** Low-Temperature Growth and Characterization of Neodymium-Substituted Bismuth Titanate Nanowires in a Highly Ordered Anodic Aluminum Oxide Template by an AC Electrodeposition Method on the Platinum Substrate for Ferroelectric Applications *Ceramics International* 42 (8) 2016: pp. 10317 – 10321.
https://doi.org/10.1016/j.ceramint.2016.03.172

10. **Wang, X.W., Ma, S.J., Wang, X.H., Ma, C., Yuan, Z.H.** Facile Conversion of Zn Nanowires to Zn Nanotubes by Heating-induced Volatilization in Nanopores of Anodic Aluminum Oxide Template *Vacuum* 132 2016: pp. 86 – 90.
https://doi.org/ 10.1016/j.vacuum.2016.07.029

11. **Wu, Y., Han, M.** Electrodeposited Fe-P Nanowire Arrays in Hard-anodic Aluminum Oxide Templates with Controllable Magnetic Properties by Thermal Annealing *Journal of Alloys and Compounds* 688 2016: pp. 783 – 789.
https://doi.org/10.1016/j.jallcom.2016.07.251

12. **Nguyen, V.H., Sichanugrist, P., Kato, S., Usami, N.** Impact of Anodic Aluminum Oxide Fabrication and Post-Deposition Anneal on The Effective Carrier Lifetime of Vertical Silicon Nanowires *Solar Energy Materials and Solar Cells* 166 2017: pp. 39 – 44.
https://doi.org/10.1016/j.solmat.2017.03.013

13. **Stepniowski, W.J., Moneta, M., Karczewski, K., Michalska-Domansk, M., Czujko, T., Johannes Buijnsters, J.G.** Fabrication of Copper Nanowires via Electrodeposition in Anodic Aluminum Oxide Templates Formed by Combined Hard Anodizing and Electrochemical Barrier Layer Thinning *Journal of Electroanalytical Chemistry* 809 2018: pp. 59 – 66.
https://doi.org/ 10.1016/j.jelechem.2017.12.052

14. **Huang, Y.S., Chen, H.Y., Liao, C.N.** Growth of Nanotwinned Cu Nanowires in Modified Anodic Aluminum Oxide Templates *Materials Letters* 288 2021: pp. 129381.
https://doi.org/ 10.1016/j.matlet.2021.129381

15. **Kikuchi, T., Onoda, F., Iwai, M., Suzuki, R.O.** Influence of Sub-10 nm Anodic Alumina Nanowire Morphology Formed by Two-step Anodizing Aluminum on Water Wettability and Slipping Behavior *Applied Surface Science* 546 2021: pp. 149090.
https://doi.org/10.1016/j.apsusc.2021.149090

16. **Kim, D.H., Kim, J.H., Jang, Y.S, Kim, J.C.** Hydrogen Production by Oxidative Steam Reforming of Methanol over Anodic Aluminum Oxide-supported Cu-Zn Catalyst *International Journal of Hydrogen Energy* 44 (20) 2019: pp. 9873 – 9882.
https://doi.org/ 10.1016/j.ijhydene.2018.11.009

17. **Qiao, N., Nong, Y., Liu, N.** Heterogeneous Catalyst of Porous Anodic Aluminum Oxide with Al Substrate Supported Metal Nanoparticles *Materials Chemistry and Physics* 225 2019: pp. 458 – 463.
https://doi.org/10.1016/j.matchemphys.2018.12.087

18. **Kozhukhova, A.E., Du Preez, S.P., Shuro, I., Bessarabov, D.G.** Development of a Low Purity Aluminum Alloy (Al6082) Anodization Process and Its Application as a Platinum-based Catalyst in Catalytic Hydrogen Combustion *Surface and Coatings Technology* 404 2020: pp. 126483.
https://doi.org/10.1016/j.surfcoat.2020.126483

19. **Yang, L., Chen, C., Rui, Z., Hongbing, J.** Anodic Aluminum Oxide Supported Pd@CeO$_2$ Catalyst for Organic Gas Pollutants Removal with an Enhanced Performance *Catalysis Today* 355 2020: pp. 602-607.
https://doi.org/10.1016/j.cattod.2019.04.065

20. **Feng, H., Elam, J.W., Libera, J.A., Pellin, M.J., Stair, P.C.** Oxidative Dehydrogenation of Cyclohexane over Alumina-supported Vanadium Oxide Nanoliths *Journal of Catalysis* 269 (2) 2010: pp. 421 – 431.
https://doi.org/10.1016/j.jcat.2009.11.026

21. **Guil-Lopez, R., Navarro, R.M., Fierro, J.L.G.** Controlling the Impregnation of Nickel on Nanoporous Aluminum Oxide Nanoliths as Catalysts for Partial Oxidation of Methane *Chemical Engineering Journal* 256 2014: pp. 458 – 467.
https://doi.org/10.1016/j.cej.2014.05.146

22. **Feng, H., Elam, J.W., Libera, J.A., Pellin, M.J., Stair, P.C.** Catalytic Nanoliths *Chemical Engineering Science* 64 (3) 2009: pp. 560 – 567.
https://doi.org/10.1016/j.ces.2008.09.027

23. **Patermarakis, G., Karayannis, H.S.** The mechanism of Growth of Porous Anodic Al2O3 films on Aluminium at High Film Thicknesses *Electrochimica Acta* 40 (16) 1995: pp. 2647 – 2656.
https://doi.org/10.1016/0013-4686(95)00250-I

24. **Patermarakis, G., Papanderadis, N.** Study on the Kinetics of Growth of Porous Anodic Al_2O_3 Films on Al Metal *Electrochimica Acta* 38 (15) 1993: pp. 2351 – 2361.

https://doi.org/10.1016/0013-4686(93)80119-K

25. **Shawaqfeh, A.T., Baltus, R.E.** Growth Kinetics and Morphology of Porous Anodic Alumina Films Formed Using Phosphoric Acid *Journal of the Electrochemical Society* 145 (8) 1998: pp. 2699 – 2706.
https://doi.org/10.1016/10.1149/1.1838701

26. **O'Sullivan, J.P., Wood, G.C.** The Morphology and Mechanism of Formation of Porous Anodic Films on Aluminum. London: Proceedings of the Royal Society of London Series A, 1970.